Korean J. Chem. Eng., 34(11), 3017-3027 (2017)
DOI: 10.1007/s11814-017-0201-3

pISSN: 0256-1115
eISSN: 1975-7220

Statistical optimization of curcumin nanosuspension through liquid anti-solvent precipitation (LASP) process in a microfluidic platform: Box-Behnken design approach

Masoud Rahimi*, Peyvand Valeh-e-Sheyda, and Hamed Rashidi**,†**

*CFD Research Center, Chemical Engineering Department, Razi University, Kermanshah, Iran
**Chemical Engineering Department, Kermanshah University of Technology, Kermanshah, Iran
(*Received 26 April 2017 • accepted 21 July 2017*)

Abstract−The paper deals with the development and optimization of curcumin nanosuspension by solvent/anti-solvent precipitation method in a microfluidic platform. A three-level Box-Behnken design was applied as an optimizing technique to investigate the effect of three independent operating variables, namely, volume ratios of anti-solvent to solvent, flow rate of drug solution, and curcumin concentration on the preferred response. In presence of PVP as the stabilizer, a nano-curcumin suspension was obtained in the range of 62-335 nm. Analysis of variance showed that the variables with the highest effect were the linear effects of the anti-solvent to solvent ratio, and its corresponding squared term. Applying response surface methodology, curcumin nanosuspension with average size of 63.12 nm can be obtained under optimum condition As: S=15, solvent flow rate of 1.0 mL/min and curcumin ethanolic concentration of 5.0 mg/mL. The prepared nanoparticles were further characterized by infrared spectroscopy, scanning electron microscopy, and X-ray diffraction tests.

Keywords: Anti-solvent, Box-Behnken, Curcumin, Microfluidics, Particle Size, Precipitation

INTRODUCTION

Many new drugs are poorly water soluble [1], and their dissolution rate can be enhanced by decreasing the particle size [2]. Recently, nanosizing of pharmaceutical compounds has shown great potential for pharmaceutical applications to enhance their bioavailability and to design suitable drug delivery systems [3-5]. While there are many techniques available for size reduction, their applicability is limited owing to poor control of the particle size, morphology, low yield, low thermal efficiency, broad particle size distribution and scalability in comparison to liquid anti-solvent precipitation (LASP) [6-8]. In recent years, supercritical anti-solvent precipitation (SASP) has been popularly employed to crystallize drugs and polymers using CO_2 as the anti-solvent [9-11]. Compared with SASP micronization technology, the solvent anti-solvent approach offers a more convenient alternative at ambient conditions without using heavy-duty equipment and high production costs [12]. Precipitation of a solid solute in LASP relies on the supersaturation of the drug solution, generated by introducing a liquid as a non-solvent [13,14].

Unlike the non-uniform distribution of the spatial concentration in macroscale solutions, micromixing on the molecular scale significantly affects the particle size distribution (PSD) of the product by LASP process [15-18]. In fact, micromixing is a key factor, which determines the degree of the supersaturation concentration of the solute, and its local spatial distribution [8]. Various methods and equipment of process intensification are being developed to gain excellent micromixing and consequently nanoparticles in precipitation processes [19-24]. Microfluidic devices, as a rapidly emerging technology, provide a series of advantages over conventional methods in terms of homogeneity with respect to concentration, temperature, and mass transfer. This leads to a better control of the precipitation step governing the particle size and its distribution, i.e., nucleation and growth [25]. The enhanced mass transfer, which lies on the microsized channel diameter, leads to a reduction of mixing times even at a laminar flow regime. The short diffusion path length [26], which is based on the large surface-to-volume ratio [27], has the most promising merits of a microfluidic system. The reactor miniaturization, controllability of the process, shorter residence time, and smaller particle size [28] with the above advantages enable microfluidics as a promising platform for nanonization of drugs.

Extensive researches have been done for development and characterization of curcumin nanoparticles, as listed in Table 1. With attention to the details in Table 1, the effects of numerous operating parameters have been evaluated on the produced particles in a classic manner. The factors affecting the size of hydrophobic curcumin particles include saturation level, flow rate of drug solution and anti-solvent, curcumin concentration, micro-reactor confluence angle, presence of stabilizers and their concentrations, resulted in precipitating with sizes mostly ranging from a few nanometers to micrometers.

In previous studies, the influence of operational variables was investigated based on a classical experimental approach. In this method, by varying one parameter at a time, the other factors are considered as constants; thus the influence of each parameter can be measured separately. The major drawback of this technique is that it

†To whom correspondence should be addressed.
E-mail: h_rashidi@kut.ac.ir

Table 1. List of literature reports available on the micro/nanonization of curcumin

Process	Solvent	Mixing device	As : S (v/v)	Particle size (nm)	Morphology	Comments	Ref.
Anti-solvent precipitation with droplet-based approach	Ethanol	T-shaped microchannel (d=250 μm)	1 : 1	200-450	Strip-shaped, needle-shaped clusters, nospheres	DI water as anti-solvent, compressed air as the gas flow pipe, air dried at 298 K	[30]
Anti-solvent precipitation	Ethanol	T-shaped microchannel (convergent angel=180° and 90°, d=300 μm)	1 : 1	105-125	Sphere	DI water as anti-solvent, SDS 0.5 wt% as surfactant, air dried at 298 K	[31]
	Ethanol	Microchannel (d=200 μm)	1 : 1	30-100	Sphere-shaped, amorphous spheres, dendritic aggregates, irregular	DI water as anti-solvent, electrospray dried	[29,33]
	Ethanol	Syringe pump	10 : 1-20 : 1	330	Lath-like	DI water as anti-solvent, vacuum dried	[32]
Anti-solvent precipitation	Ethanol	Microchannel (confluence angle of 45°, 90° and 135°, d=800 μm)	10 : 1	181-350	Amorphous particles of irregular shapes	DI water as anti-solvent, freeze-dried	[34]
Anti-solvent precipitation	Ethanol	Microchannel d=800 μm (confluence angle of 45°, 90° and 135°, d=800 μm)	10 : 1	77-488	Agglomerates	DI water as anti-solvent, freeze-dried	[35]
Evaporative precipitation of nanosuspension (EPN)	Ethanol	Syringe pump	10 : 1-20 : 1	150	Needle-like	Hexane as anti-solvent, stirring speed= 200-1000 rpm, vacuum dried	[32]

neglects any possible interaction between the factors, and this may affect the real optimum response. Besides, the traditional experiments require more effort, time, and materials when preparing curcumin nanoparticles. In addition, no general validity rules have been presented from the ones experimentally studied. As a case in point, various particular morphologies and dispersion like sphere, needle, amorphous and strip-shaped with different characteristics have been reported [29-32].

Response surface methodology (RSM) is a widely practiced approach that provides large amounts of information from a small number of experiments. It also allows the user to observe the effects of distinguishing variables and their combinations of interactions on the defined response. However, the selection of experimental design is based on the objectives of the experiment and the number of parameters to be investigated [28]. Comparison of response surface methodologies (Doehlert matrix, Box-Behnken (BBD), central composite, and three-level full factorial design) illustrates that the BBD requires less treatment with relatively high quality predictions than the other designs. BBD is useful in introductory investigations where the aim is to determine variables that can be fixed, or eliminated in subsequent studies. It is also highly effective in avoiding experiments carried out under extreme conditions, for which undesirable results might happen. However, they are not suggested for situations in which the responses are at the extremes [36].

In the present investigation, curcumin nanoparticles were obtained in a microfluidic platform, focusing on a controlled nano-precipitation process. A computer-aided technique using BBD was first introduced as a predictive model, describing the main effects and possible interactions of the experiment process parameters on the size of curcumin nanoparticles. Moreover, using various analytical instruments, the physical characteristics of the precipitated particles were evaluated before and after processing. On the next stage, BBD was applied as an optimizing technique to find a stable nanosuspension formulation for nano-precipitation of curcumin particles in designed microfluidic platform.

MATERIALS AND METHODS

1. Materials

Raw curcumin ($C_{21}H_{20}O_6$) with a mean particle size of 28.96 μm (95%) and Polyvinyl pyrrolidone (PVP, $C_6H_9NO)_n$ were procured from Merck-Schuchardt, Germany and used without further purification. Ethanol, as the solvent, was purchased from Mojallali Chemical Laboratories, Iran. The deionized (DI) water (Milli-Q, Millipore, Singapore) was used in all experiments.

2. Apparatus and Experimental Procedure

The first step of the precipitation experiments was the preparation of original curcumin solutions in ethanol at the predetermined concentrations of 0.05, 2.52, and 5 mg/mL. The organic solution was then filtered through a syringe filter with a pore size of 0.45 μm and

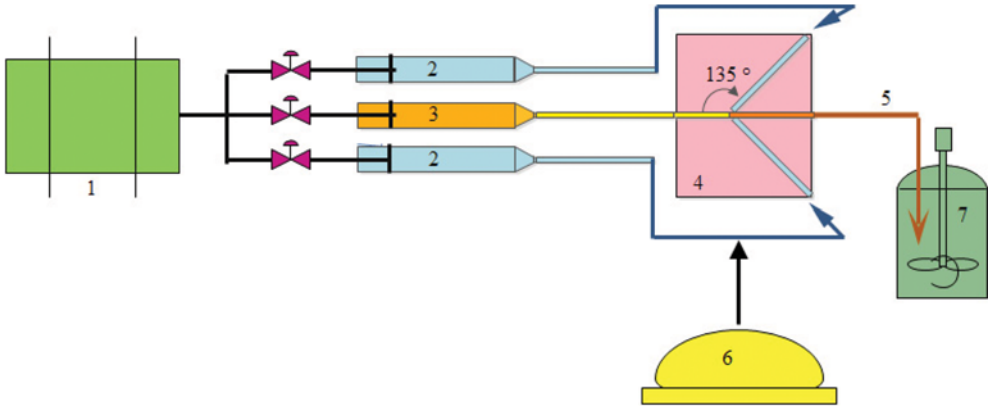

Fig. 1. Experimental apparatus for the liquid anti-solvent precipitation.

1. Electric motor
2. Syringe pump (anti-solvent inlet)
3. Syringe pump (solvent inlet)
4. Microchannel (micro mixer)
5. Outlet stream
6. Lamp
7. Analysis chamber

Table 2. Coded and real values of the factors for three level Box-Behnken statistical design

Independent variables	Symbol	Uncoded variable level		
		Low (−1)	Center (0)	High (+1)
As : S ratio	x_1	2.00	8.50	15.00
Drug solution flow rate (mL/min)	x_2	1.00	7.00	13.00
Curcumin concentration (mg/mL)	x_3	0.05	2.52	5.00

sonicated (bath sonicator, Tecno-Gaz) for 2 min to get a transparent solution. The non-solvent solution was prepared with 0.03% w/v by dissolving a definite amount of water-soluble stabilizer, PVP, in 100 mL of DI. The aqueous solution of surfactant was homogenized continuously at room temperature in a mixer for 1 h. Before processing, the solution was filtered through a 0.22 μm syringe filter to remove any possible particulate impurities.

The microfluidic device was fabricated in-house using poly-methyl methacrylate. The channels were made with a precise mill cutter, in a circular shape with diameter of 800 μm and length of 3 cm. Continuous-flow nano-precipitation of curcumin nanosuspension was carried out in a micromixer setup, illustrated in Fig. 1. As presented, by dividing the anti-solvent flow into two jets, a symmetric flow rate was provided, as the non-solvent solutions impinged at the junction part.

In brief, the organic and anti-solvent solutions were filled separately with syringes. A motorized syringe pump, as an injector, adjusted the solvent and anti-solvent flow rates at appropriate operating levels of 1 : 2-1 : 15 (v/v) to achieve various As : S ratios. Next, the prepared curcumin solution was injected by the syringe pump at a fixed flow rate of 1 to 13 mL/min. Under microfluidic mixing of the two media during 1 min of injection, the prompt solid precipitation of the dissolved drug was observed at the microchannel outlet flow. The collected nanosuspension from the outflow of the microfluidic device was stirred continuously at 1,500 rpm with a propeller mixer at a constant room temperature of 25 °C, to allow complete crystal growth. The stirred vessel volume varied between 100 and 600 mL, depending on the amount of the anti-solvent used. In the next step, the obtained suspensions were instantly frozen in the liquid nitrogen and then freeze dried for 48 h to eliminate any water and organic solvent and hold dispersed powders.

3. Design of the Experimental Method

A three-factor, three-level Box-Behnken factorial design was adopted to statistically evaluate the main effects, interaction effects, and quadratic effects of anti-solvent volume ratio to solvent (As : S (x_1)), solvent flow rate ((x_2) mL/min), and curcumin concentration ((x_3) mg/mL) on produced particle size (Y). Table 2 presents the coded and real values of the factors for the 3^3 Box-Behnken design (BBD).

The BBD was specifically selected, since it requires fewer runs than a central composite design in cases of three or four variables. In addition, the effects of individual parameters as well as their relative importance can be considered. It is also economical and specifically useful when it is expensive to conduct the required experimental runs. This cubic design is beneficial for the examination of quadratic response surfaces with a second-degree polynomial model, and can be used in process optimizing using a relatively small number of experimental runs [37-39]. The number of experiments required in BBD is determined based on $N=k^2+k+c_p$, where N, k, and c_p are the number of experimental runs, factor number, and the number of replications at the center point, respectively [40]. In the current study, the values of N, k, and c_p were 15, 3, and 3, respectively. Applying MINITAB (version 14), a design matrix comprising 15 experimental runs was constructed, as shown in Table 3. The levels of the independent variables along with their low, medium, and high values were selected based on preliminary experiments (see also Table 2). The relationship between the coded and real values can be expressed using Eq. (1):

$$X_i = \frac{x_i - A_0}{\Delta x_i} \quad (1)$$

Table 3. Coded and actual values of the independent variables in the Box-Behnken design matrix with the experimental and predicted values of curcumin particle size

Test code	Coded variables[a]			Actual values			Experimental particle size		Predicted particle size
	X_1	X_2	X_3	x_1	x_2	x_3	Z-average (nm)	PdI	Z-average (nm)
BB1	−1	−1	0	2	1	2.52	276.8	0.136	297.98
BB2	−1	0	−1	2	7	0.05	335.5	0.054	314.18
BB3	−1	0	1	2	7	5	342.8	0.173	315.95
BB4	−1	1	0	2	13	2.52	232.0	0.192	258.96
BB5	0	−1	−1	8.5	1	0.05	266.2	0.093	259.20
BB6	0	−1	1	8.5	1	5	102.4	0.105	100.93
BB7	0	0	0	8.5	7	2.52	120.0	0.306	123.95
BB8	0	0	0	8.5	7	2.52	135.0	0.306	123.95
BB9	0	0	0	8.5	7	2.52	125.5	0.306	123.95
BB10	0	1	−1	8.5	13	0.05	119.8	0.211	125.57
BB11	0	1	1	8.5	13	5	145.2	0.091	156.50
BB12	1	−1	0	15	1	2.52	142.6	0.187	138.49
BB13	1	0	−1	15	7	0.05	197.6	0.262	220.13
BB14	1	0	1	15	7	5	74.03	0.146	91.02
BB15	1	1	0	15	13	2.52	134.9	0.026	99.47

[a]The coded variables X_1, X_2, and X_3 were calculated from their respective real values x_1, x_2, and x_3

where, X_i and x_i represent the coded and real values of the independent variables, respectively, and A_0 and Δx_i represent the real value of the independent variables at the center point and step change of x_i, respectively.

The response variable was fitted by a second-order model to correlate the size of precipitated particles to the independent variables. The general form of the second-degree polynomial equation is of the following form:

$$y = \beta_0 + \sum_{i=1}^{t} \beta_i x_i + \sum_{i=1}^{t} \beta_{ii} x_i^2 + \sum_{i<j}^{t} \beta_{ij} x_i x_j \quad (2)$$

where y is the predicted response associated with each factor; β_0 is a constant offset term; x_1, x_2 and x_3 independent variables; β_i are the linear main effects; β_{ii} are the quadratic main effects and β_{ij} are interaction coefficients between x_i and x_j that influence the response variable [41].

Statistical ANOVA was performed to statistically analyze the significance of the process parameters. The analysis included the determination coefficient (R^2, agreement between the experimental results and predicted values obtained from the model), standard error of estimate, sum of squares of the errors, the model F-value (Fisher variation ratio, the ratio of mean square for regression to mean square for residual), and p value. The corresponding BBD and experimental data are shown in Table 3.

CHARACTERIZATION OF PRODUCTS

1. Dynamic Light Scattering (DLS) and Zeta Potential Measurements

The mean particle size of the freshly precipitated curcumin particles was determined by dynamic laser light scattering technique (Nano-Zeta sizer, Malvern Instruments, Nano series, Nano-ZS, UK), equipped with Malvern PCS software (version 1.27). The refractive index of the suspension medium was measured in 25±0.1 °C by a refractometer, (Model RE4OD, Metter Toledo) with a precision of 0.0001 refractive index units.

The investigated parameters were the average of particle size diameter (Z-Average), and the polydispersity index (PdI). In summary, the Z-average size, also known as the "cumulants mean," denotes the size of spherical, reasonably narrow monomodal samples. The PdI is an important parameter in nanosuspension technology, since it indicates the width of particle size distribution, as well as the long-term stability of nanosuspension. For broader distributions, where the PdI is over 0.5, a distribution analysis should be also utilized to ascertain the peak positions (Zetasizer nano series user manual, 2004.).

The zeta potential (ζ) was also calculated by the zeta sizer nanoparticle analyzer (Malvern Instruments, Nano series, Nano-ZS, UK) from electrophoretic mobility using Henry's equation [42].

$$U_E = 2\varepsilon\zeta f(K\alpha)/3\eta \quad (3)$$

U_E is the electrophoretic mobility, ε is the dielectric constant of the suspending medium, η is the viscosity of the medium, K is the Debye-Hückel parameter, and f ($K\alpha$) is a correction factor that considers the thickness of the double layer and particle diameter (α). The K unit is a reciprocal length, and 1/K generally represents the electrical double layer thickness. Measurement was carried out for each sample twice at 25 °C, and no dilution was performed before measurements. In this regard, the initial particle size of the fresh curcumin powder was obtained as 28.96 μm with PdI of 0.817, which is technically outside the nanoparticle size range.

2. Scanning Electron Microscopy (SEM)

SEM analysis was carried out to examine the surface structure of the freeze-dried curcumin nanoparticles and also to verify the particle size analysis, qualitatively. To record SEM pictures, an AIS 2100 microscope 86 from Seron was used. The dried nanoparticles

were sputter coated with a thin layer of pelco gold palladium at room temperature to improve thermal conductivity.

3. X-ray Diffraction Studies (XRD)

X-ray diffraction measurements of the freeze-died curcumin samples were performed on a Philips X'Unique II, X-ray diffractometer with copper spectrum (with a wavelength of 1.54 angstrom) to detect the crystallinity of curcumin. The samples were analyzed over the angle range of 5° to 55° on the 2θ scale at a step size of 0.05/sec.

4. Fourier Transform Infrared Spectroscopy (FT-IR)

To evaluate the molecular states of raw curcumin and the final nanosized curcumin, Fourier transform infrared (FT-IR) analysis was carried out using an IR Prestige-21 FT-IR spectrophotometer (Shimadzu, Japan). For that, samples were diluted with KBr mixing powder at 1%, and pressed into suitable-size disks for measurement. FT-IR transmittance and absorbance spectra were recorded in the wavelength region of 500-4,000 cm^{-1} with resolution of 8 cm^{-1}.

5. Differential Scanning Calorimetry (DSC)

The DSC thermal profile of the optimal sample was determined using a thermogravimetric analyzer (DSC-500-B) at a heating rate of 10 °C/min using a nitrogen purge. Samples were heated from 25 to 250 °C and placed in aluminum pans. The melting points and their enthalpies were then calculated by the software.

RESULTS AND DISCUSSION

1. Model Fitting and Statistical Analysis

The measured values of curcumin particle size along with corresponding predicted values obtained from the 15 runs are listed in Table 3. Experimental values of particle size were found in the range of 74.03 nm (BB14) to 342.8 nm (BB7), while the predicted size was and 91.02 nm and 315.95 nm, respectively.

Applying the second-degree polynomial model, the effects of independent variables were evaluated on selected dependent variables. As a starting point for construction of the model, the statistically insignificant factorial terms were eliminated by step-wise backward method (e.g., x_1x_2 was removed because the x_1x_2 interaction was not significant). Finally, the quadratic equation obtained for the curcumin particle size (y) was given by:

$$y=462.087-37.219\,x_1-11.295\,x_2-48.042\,x_3 +1.770\,x_1^2+5.974\,x_3^2-2.034\,x_1x_3+3.185\,x_2x_3 \quad (4)$$

where y is the average size of precipitated particles (nm), x_1 anti-solvent to solvent ratio, x_2 curcumin solution flow rate, and x_3 initial concentration of curcumin solution (mg/mL). A positive value for the measured response indicates the synergistic effect, whereas a negative value represents the antagonistic effect between the factor and the response [43]. As an illustration, the main effects of x_1, x_2, and x_3 have an inverse relationship with the response, y. Furthermore, in quadratic equation of y, the main effects of x_1, x_2, and x_3 demonstrate the average results of changing one variable at a time from its low-level to high level, while the interaction terms x_1x_3, and x_2x_3 represent how the size of precipitated particles varies as two variables are changed at the same time [28].

The significance of the fitting of the quadratic model for the response, y, was assessed by carrying out one way analysis of variance (ANOVA). The statistical significance was set at 95% of confidence level ($p<0.05$). It is well known that a value of p less than or equal to α level ($\alpha=0.05$) indicates that the effect for the corresponding term is statistically significant. However, value greater than 0.10 means that the model terms are not significant. The results of ANOVA for the measured response, y, are listed in Table 4.

From the regression model of response, the linear coefficients of anti-solvent to solvent ratio (x_1), solvent flow rate (x_2), initial concentration of curcumin solution (x_3), and the quadratic terms of

Table 4. Coefficients of the quadratic model and ANOVA for factors and their Interactions from Box-Behnken

	Coefficients	t-Stat	P-value			
Constant	461.490	13.005	0.000			
x_1 (As : S ratio)	−37.027	−6.173	0.000			
x_2 (solvent flow rate (mL/min))	−11.295	−4.179	0.004			
x_3 (drug concentration (mg/mL))	−47.649	−3.181	0.015			
x_1 x_1	1.758	5.480	0.001			
x_3 x_3	5.896	2.664	0.032			
x_1 x_3	−2.034	−2.505	0.041			
x_2 x_3	3.185	3.621	0.008			
R-Sq = 95.4%	R-Sq(adj)=90.9%					
Source	DF	seq SS	adj SS	adj MS	F	$F_{\alpha=0.05}$	p
Regression	7	9967.2	99672.4	14238.9	20.89	3.79	0.000
Linear	3	62029	38421.7	12807.2	18.79	4.35	0.001
Square	2	24413	24412.8	12206.4	17.91	4.74	0.002
Interaction	2	13231	13230.9	6615.4	9.70	4.74	0.010
Residual Error	7	4772	4771.8	681.7			
Lack-of-Fit	5	4657	4656.6	931.3	16.17	3.97	0.059
Pure Error	2	115	115.2	57.6			
Total	14	104444					

the ratio of anti-solvent to solvent and curcumin concentration in organic solution (x_1x_1 and x_3x_3) are found as significant ($P<0.05$). However, the variables with the highest effect are the linear effects of the anti-solvent to solvent ratio, and its corresponding squared term. Moreover, the two interaction coefficients of As : S and curcumin ethanolic solution (x_1x_3), and the interactive effect of solvent flow rate and concentration of curcumin solution (x_2x_3) have p values less than 0.05. In this case, the interaction of x_1x_3 as well as x_2x_3 has significant impact on the size of curcumin particles in microfluidic precipitation. The corresponding p-value of 0.000 in Table 4 further confirms that the model was suitable for use in the current experiment.

Another important statistic parameter in ANOVA table is the F-value, listed in Table 4. As seen in the table, the F-values of all factors and interactions are greater than the extracted F-values of tables with 95% confidence ($F_{\alpha=0.05}$). This means that the variance of each factor and their interactions are significant compared to the variance of error and that all of them have an important effect on the response. As an illustration, the F-value for the model was found to be 20.89, which is much higher than the tabulated F-value ($F_{95,0.05}$) of 3.79. Such a large value of F for the model indicates that the predicted second-order polynomial is highly significant to a 95% confidence level. Besides, the value of lack of fit 0.059 indicates that there is only 5% chance that the lack of fit of F-value could occur due to noise, meaning that lack of fit is not significant relative to the pure error. Based on this table, the coefficient of determination (R^2), and the adjust coefficient of determination (adj-R^2) of the predicted model are observed as 0.95 and 0.90, respectively. Thus, the predicted model can explain 95% of the variability in the response.

Overall, statistical analysis showed that the experimental values fitted well with the predicted ones. In this regard, the accuracy and general availability of the polynomial established model were adequate for further optimization of particle size predictions in LASP process.

1-1. Selection of Optimal Conditions with Response Surface Graphs

The three-dimensional response surface and two-dimensional contour graphs are the graphical representations of regression functions. While the former describes the sensitivity of response value toward the change of variable, the latter illustrates the significance of interactions between the corresponding variables [44,45]. Fig. 2 and Fig. 3 represent the response surface plots for optimization of dependent variable. The optimal values of the variable were selected based on the lowest size of precipitated curcumin particles at the microfluidic outlet. All of the graphs were constructed by keeping one independent variable at a constant level, which was the coded zero level, while the other two independent variables varied within the experimental ranges. The coordinates of the central point within the minimum contour levels in each of the given figures represent the optimum values of the respective parameters.

The response surface and contour plots in Fig. 2(a) and (b) show the size of precipitated curcumin particles as a function of As : S ratio, and initial concentration of curcumin solution when the flow rate

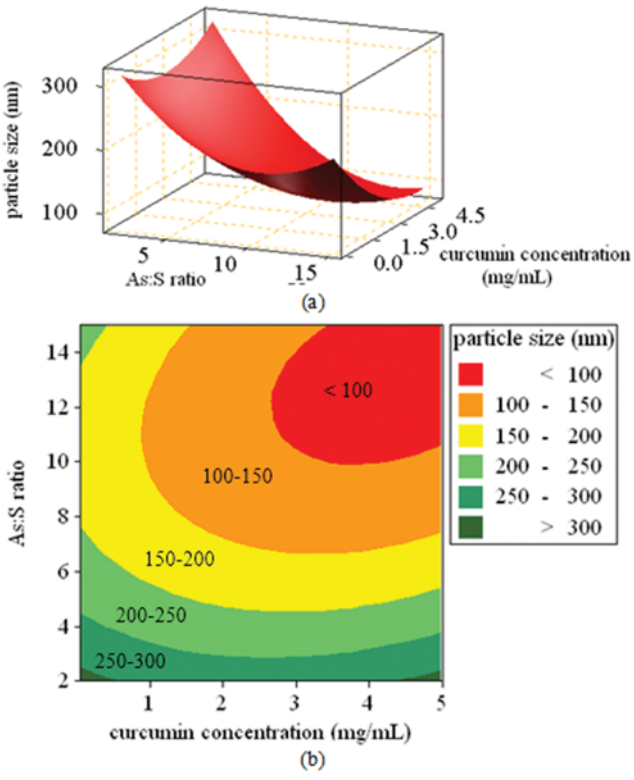

Fig. 2. (a) Response surface, and (b) contour graphs of As : S ratio and initial concentration of curcumin solution on size of precipitated particles.

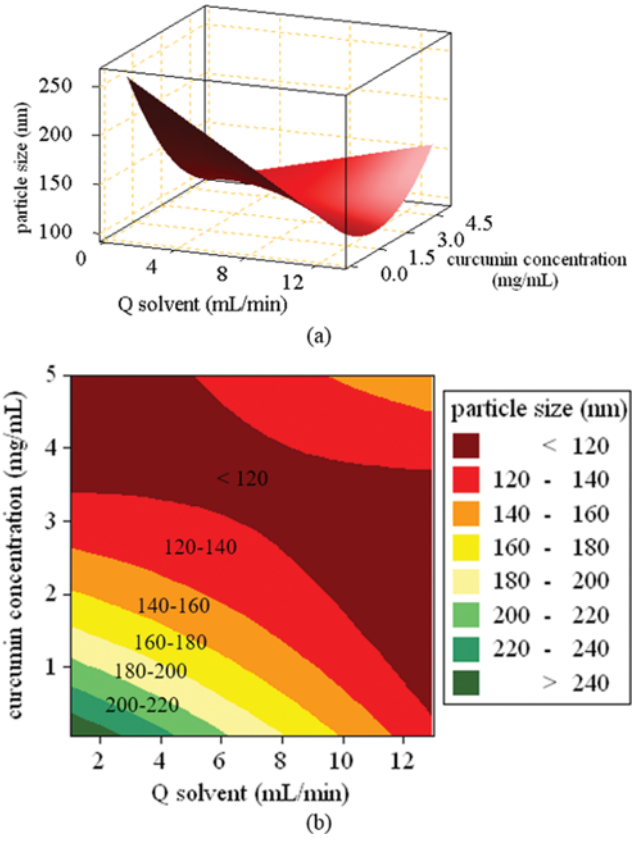

Fig. 3. (a) Response surface, and (b) contour graphs of precipitated particle size as a function of curcumin initial concentration and solvent flow rate.

of solvent is fixed at (0) level (7 mL/min). It is clear that the size of the curcumin particles varied between 100 to 300 nm. In this case, the impact of As : S is more significant than the curcumin initial concentration. In addition, the results in Fig. 2 indicate an inversely proportional relationship between the amount of anti-solvent to solvent ratio and the particle size. As the amount of DI water to the curcumin solution increases from 2.0 to 15.0, the mean particle size is found to decrease significantly. There are a few reasons for this observation. Based on the equations presented for the rate of nucleation in the literature [46], a greater amount of anti-solvent should lead to a greater nucleation rate, and hence smaller nuclei. Once the nuclei are formed, growth occurs simultaneously. For further growth, more anti-solvent amount increases the diffusion distance for growing species, and thus diffusion becomes the limiting step for nuclei growth [47]. That is why faster precipitation of the drug into nanoparticles would occur at higher values of As : S ratio, resulting in reduction the size of precipitated curcumin particles.

The impact of curcumin initial concentration was also investigated in Fig. 2(a) and (b). At low values of As : S, the particle size initially decreased with increase in concentration of curcumin solution. However, an opposite trend was observed when curcumin initial concentration exceeded to a certain level of 3 mg/mL. This result can be interpreted by considering the dependency of the nucleation rate on the concentration of curcumin solution in two opposing ways. Upon mixing with the anti-solvent, higher concentrations of drug solution lead to a greater supersaturation, leading to a faster nucleation rate, and thereby smaller particles. Thus, a high rate of nucleation stands for the formation of a large number of nuclei that increases the number of crystals and makes each particle smaller. In contrast, high supersaturation can also speed up agglomeration through the greater chance of particle collision to generate large particles [32,48]. On the other hand, at a higher curcumin concentration, a large number of nuclei are formed at the interface of two phases. This may lead to agglomeration and thus, formation of larger particles. Those nuclei obstructed the further diffusion of drug molecules from the solvent to anti-solvent, resulting in non-uniform supersaturation [49], and thus formation of the larger drug particles. These trends have been consistently observed in the literature of previous studies [12].

In the present study, higher values of As : S ratio, and drug concentration resulted in smaller particle size for curcumin. This indicates that in our study nucleation prevailed over agglomeration at high drug concentrations.

Fig. 3 illustrates the effects of initial concentration of curcumin solution, and solvent flow rate on curcumin particle size at a fixed As : S ratio of 8.5. The volumetric flow rate, Q, was varied from 1 mL/min to 7 mL/min, then to 13 mL/min, and the corresponding values of Reynolds number (Re No.) increased from 21 to 151 then to 280. The value of Re number was calculated according to the following equation:

$$\mathrm{Re} = \frac{\mathrm{Qd}}{\mathrm{A}\nu} \tag{5}$$

where d is the diameter of the microfluidic (m), ν is the kinematic viscosity (m^2/s), Q is the volumetric flow rate (m^3/s), and A is the microfluidic cross-sectional area (m^2). The microchannel diameter of the 0.8 mm, and the kinematic viscosity of 1.239×10^{-6} m^2/s for ethanol were used to calculate the value of Re number. Note that since the density and viscosity of the mixture change during LASP processes, the Re number at the solvent inlet was taken as the reference variable to investigate the mixing performance.

Considering Fig. 3(a), direct relation of $Q_{solvent}$, and drug concentration on the size of precipitated particles is clear. At low flow rates of curcumin solution (<4 mL/min), the average size of curcumin particles decreased by 100% from 240 nm to 120 nm, indicating that a considerable amount of molecular diffusion between water and ethanol occurred at the very beginning of the contact of two inlet streams [31]. Accordingly, the effect of the concentration difference, as the driving force of liquid-liquid mass transfer, is dominant when the bulk flow velocity is small. In contrast, at high flow rates of curcumin solution (Q>12 mL/min, Re>280), the average size of curcumin particles would slightly decrease to less than 120 nm, as the curcumin concentration decreased.

It seems that in spite of decrease in diffusion between the two streams, with increasing Re number, a narrower particle size distribution would occur, which corresponds to a shorter residence time in the microfluidic device. This can be explained based on the fact that at low concentrations of curcumin solution, increasing the flow rate increases the jet velocity, the Re number, and shear forces, resulting increase in the extent of mixing between the drug solution and the anti-solvent per unit time [32]. Thus, the initial mixing quality, at high Re values, causes a higher consumption of free curcumin molecule in the mixture, and therefore, more crystal nuclei can be generated. Consequently, the molecules left for the growth of each particle become less, leading to a slower growth rate. The visualization investigations of Wang et al. [31] in T-shaped microchannels coincide well with our statistical results.

Similar observation was also depicted in the two-dimensional contour plot of Fig. 3(b). Regarding the details in contour plots of Figs. 2(b) and 3(b), during the development of nanosuspension, interaction of curcumin concentration with the other two independent variables including As : S ratio and flow rate of solvent, was also significant.

In general, it can be predicted that optimal values of the curcumin particles are achieved at both low and high values of Re No. than at medium values. Moreover, the average size of the curcumin nanoparticles can be adjusted in a fully controlled manner by simply changing the initial drug concentration. This was also found in previous studies [30]. Furthermore, the interaction effects of As : S ratio and $Q_{solvent}$ were not showing any significant impact on the size of precipitated particles.

1-2. Method Validation and Application

Response optimization was carried out by combination of input parameters [50] to reduce the average size of precipitated curcumin particles in designed microfluidic platform. Then, the optimal values were computed and the suitability of the model equation was tested for predicting optimum response value. The values of the process parameters giving the minimum particle size are shown in Table 5. As can be seen, the optimum value was determined as 63.12 nm at an optimized As : S ratio, solvent flow rate and curcumin concentration level of 15.0, 1.0 mL/min and 5.0 mg/mL, respectively.

Table 5. Values of process parameters for optimum particle size

Parameter	Coded value	Actual value
Dependent parameter		
y	-	63.12
Independent parameters		
x_1 (As : S ratio)	+1	14.97
x_2 (drug solution flow rate (mL/min))	−1	1.00
x_3 (curcumin concentration (mg/mL))	+1	5.00

To validate the accuracy of the model in size prediction of precipitated particles by LASP method, experimental measurements were performed at above-mentioned levels.

Considering the DLS results, the particle size of the as-prepared sample was obtained as 62.00 nm. The good fitting of the experimental and predicted values further supports that the full quadratic polynomial model used in the current study is adequate for describing the LASP process of curcumin nanosuspension in microfluidic reactors. Fig. 4 illustrates the particle size and cumulative size distribution of curcumin nanoparticles predicted by BB design. Note that the horizontal axis is plotted on a log-scale, whereas the vertical axes indicate the percentage of cumulative distributions and the particle size in terms of intensity, respectively. Suppose the particles are spheres, other distributions including either volume or number are regularly estimated by an appropriate mathematical manipulation generated from intensity [51]. From the figure, 80% of the amounts of particles are clearly at or below 40 nm. Thus, the RSM technique can be usefully applied to optimize the size of curcumin nanoparticles in the designed microfluidic reactor by employing the LASP process.

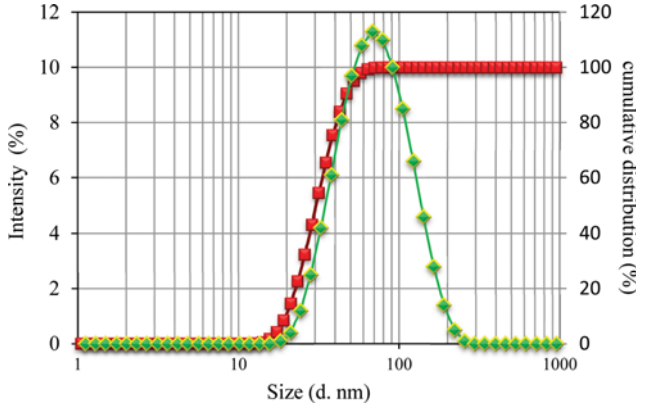

Fig. 4. Cumulative and particle size distribution of curcumin nanosuspension obtained from validation test.

2. Characterization of Nanoparticles

2-1. Zeta Potential

Detailed information related to the zeta potentials of curcumin nanosuspension prepared by LASP microfluidic process is presented in Fig. 5. The zeta potentials of all samples exhibit negative surface charge, which is attributed to the carbonyl group of PVP capable of donating electron. Besides, as the stabilizer molecules adsorb

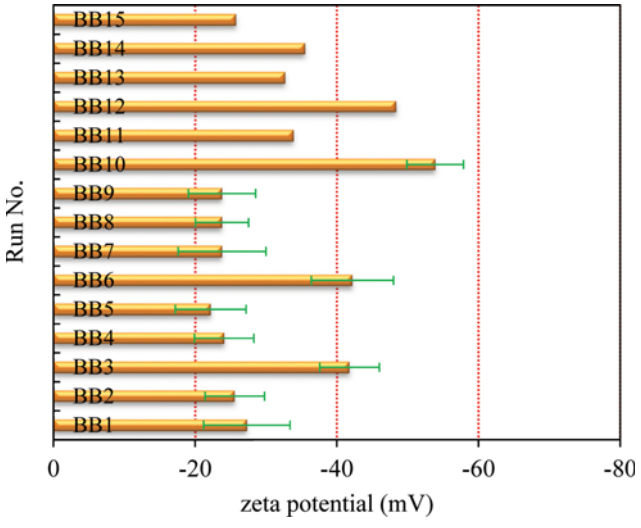

Fig. 5. Zeta potential values of nanoparticles prepared in designed microfluidics by LASP method.

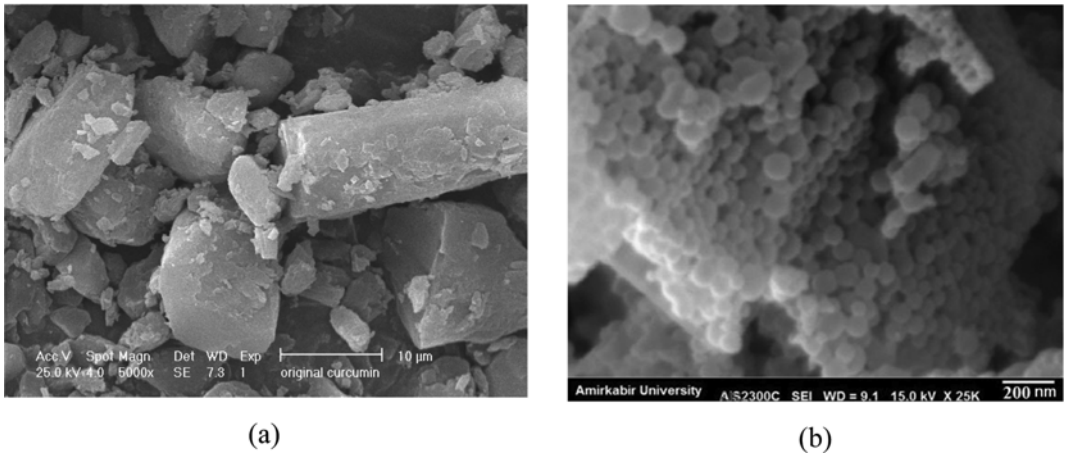

Fig. 6. SEM photographs of curcumin nanoparticles prepared by LASP (a) the raw material (b) the optimum Box-Behnken particle precipitated by LASP (BB14).

onto the surface of curcumin nanoparticles, the ionization of phenolic functional group in an aqueous environment imparts a negative charge to the curcumin particles to prevent agglomeration during 15 min after curcumin precipitation. This negativity suggests a favorable interaction between PVP and curcumin molecules. The same ranges of zeta potentials were reported by other researchers for curcumin-PVP nanoparticles [52]. A spherical shape of curcumin nanoparticles may be a result of adequate stabilization of curcumin nanosuspensions through hydrogen bonding with curcumin molecules.

2-2. Scanning Electron Microscopy (SEM)

Fig. 6 shows the SEM image of as-purchased and freeze-dried curcumin powder obtained from BB14 suspension under optimum condition. It is evident that the primary particles of raw curcumin possess large and irregular morphology with different sizes. In case of BB14, the nanoparticles were almost spherically pearl-like with a uniform size distribution in the range of 50-80 nm, confirmed by DLS measurements. Although the 0.03% w/v PVP may provide a suitable steric hindrance for inhibiting aggregation and particle growth, the aggregation of particles during freeze-drying is inevitable.

Morphological behavior of curcumin particles when precipitated from its ethanolic solution in the presence of polymeric stabilizers such PVP has also been confirmed by Thorat et al. [52]. They also reported that curcumin particles precipitated with PVP clearly look like aggregates, formed by the assembly of several spherical nanoparticles.

2-3. X-ray and FTIR Analysis

The solid structures of the raw and processed curcumin precipitated from BB14 Box-Behnken design are exhibited in Fig. 7. As shown, the X-ray diffractograms of pure curcumin contain characteristic peaks at diffraction angle of 2θ at 7.86, 8.78, 12.18, 14.46, 15.84, 17.14, 21.08 *etc.* [54]. This reveals that the raw curcumin is relatively present as a crystalline form. In contrast, the crystalline peaks are not clearly found in the diffraction patterns of the sample BB14, demonstrating that curcumin nanoparticles are relatively in amorphous state.

The FTIR spectrum of the raw and precipitated curcumin nanoparticles (BB14) was compared in Fig. 8. As seen, the identical FT-IR spectrum demonstrates that the chemical structure of the precipitated nanoparticles was not changed after the precipitation process in microfluidic channel. However, the FT-IR spectrum of the freeze-dried curcumin nanoparticles showed some small differences in the range of 1,710-880 cm^{-1} (C-O stretching), due to the employment of the PVP stabilizer during LASP process.

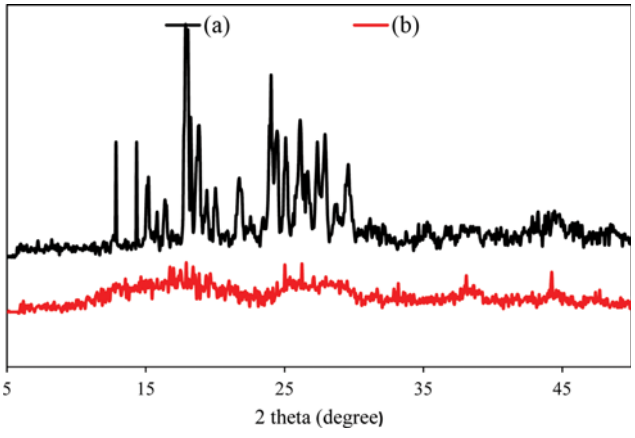

Fig. 7. XRD of (a) raw curcumin (b) optimum curcumin nanoparticle (BB14).

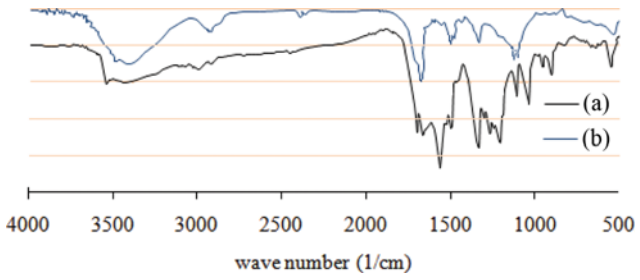

Fig. 8. FTIR spectra of curcumin particles precipitated (a) pure powder (b) optimum nanoparticle (BB14).

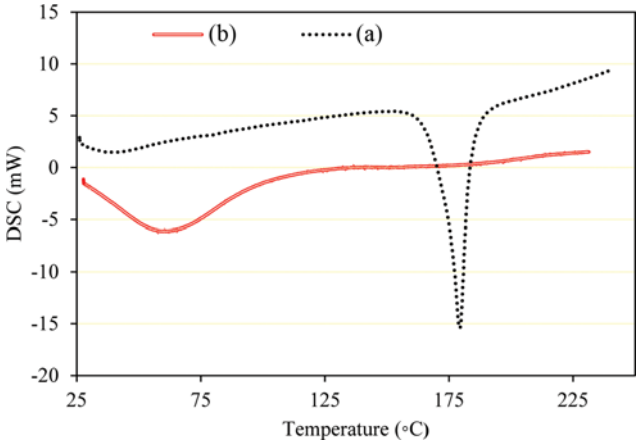

Fig. 9. DSC thermograms of (a) raw curcumin, and (b) processed curcumin nanoparticles (BB14).

2-4. DSC Analysis

DSC thermograms of the raw and precipitated nanoparticles of BB14 are illustrated in Fig. 9 to examine the crystallinity. According to this figure, the original curcumin exhibits a sharp peak depression at 179.3 °C, corresponding to its melting point. In case of the processed curcumin, this endotherm is broadened and shifted completely to a lower temperature at 55.7 °C. This depression of melting point is attributed to the reduction of the curcumin particle size down to the nanosized range, as described by the Gibbs-Thomson equation [54,55]. In addition, the fast nucleation rate in the molecular level prevents crystallization of curcumin molecule, resulting in imperfect crystals [56]. The amorphous state of these particles was also confirmed by comparing the XRD spectra of the processed curcumin.

CONCLUSIONS

This study focused on optimizing the curcumin nanosuspension through microfluidic precipitation process using response surface

methodology. The main issue was to find the effects of anti-solvent to solvent ratio (x_1), solvent flow rate (x_2) and initial concentration of curcumin solution (x_3) on the size of curcumin nanosuspensions. The significance of the fitting of the quadratic model for the response was statistically assessed by carrying out one way ANOVA.

It was found that the linear coefficients of x_1, x_2, and x_3 have an inverse relationship with the response. The relative order of importance of these factors was As : S ratio, solvent flow rate, and curcumin concentration, respectively. Moreover, the interaction the quadratic terms of x_1x_1, x_1x_3 as well as x_2x_3 had significant impact on the size of curcumin nanosuspension in microfluidic precipitation. However, the interaction effects of As : S ratio and $Q_{solvent}$ were not showing any significant impact on the size of precipitated particles.

In general, when the flow rate of solvent was fixed at (0) level, the impact of As : S was more significant than the curcumin initial concentration. There was also an inversely proportional relationship between the amount of anti-solvent to solvent ratio and the particle size. Thus, the faster precipitation of curcumin into nanoparticles would occur at higher values of As : S ratio, resulting in reduction of the size of precipitated particles. Furthermore, the optimal values of the curcumin particles were achieved at both low (Re< 21) and high (Re>280) values of Re No. than at medium values.

Based on the results of second-order quadratic model in Box-Behnken design, the average particle size of 62.00 nm was obtained at an optimized As : S ratio of 15, solvent flow rate of 1.0 mL/min and curcumin ethanolic concentration of 5.0 mg/mL. Finally, the accuracy and general availability of the polynomial established model demonstrates that this methodology along with microfluidics, as a promising platform, could be implemented for nanonization of other poorly water-soluble drugs, which can be precipitated by the LASP technique.

NOMENCLATURE

ANOVA : analysis of variation
API : active pharmaceutical ingredients
AS : S : anti-solvent to solvent volumetric ratio
BBD : Box-Behnken design
C_p : the number of replications
d : diameter of the microchannel [m]
DF : degrees of freedom
h : hour
K : Debye-Hückel parameter
k : factor number
LASP : liquid anti-solvent precipitation
mV : milli volt
Mol.wt. : molecular weight
N : the number of experimental runs
PdI : polydispersity index
PSD : particle size distribution
PVP : poly(vinylpyrrolidone)
Q : volumetric flow rates of feed [mL/min]
Re No.: reynolds number
RSM : response surface methodology
rpm : round per minute
v : volume
w : weight
y : the predicted response [nm]

Greek Symbols

α : particle diameter
β_0 : constant offset term
β_i : the linear main effects
β_{ii} : the quadratic main effects
β_{ij} : interaction coefficients between x_i and x_j
ε : dielectric constant
ζ : zeta potential
η : the viscosity of the medium
ν : the kinematic viscosity [m^2/s]

REFERENCES

1. C. A. Lipinski, *Am. Pharm. Rev.*, **5**, 82 (2002).
2. A. A. Noyes and W. R. Whitney, *J. Am. Chem. Soc.*, **19**, 930 (1897).
3. L. Lindfors, S. Forssén, J. Westergren and U. Olsson, *J. Colloid Interface Sci.*, **325**, 404 (2008).
4. I. Pasquali, R. Bettini and F. Giordano, *Adv. Drug Delivery Rev.*, **60**, 399 (2008).
5. I.-S. Kim and S.-H. Kim, *Int. J. Pharm.*, **245**, 67 (2002).
6. M. E. Matteucci, B. K. Brettmann, T. L. Rogers, E. J. Elder, R. O. Williams Iii and K. P. Johnston, *Mol. Pharmaceutics*, **4**, 782 (2007).
7. J.-F. Chen, J.-Y. Zhang, Z.-G. Shen, J. Zhong and J. Yun, *Ind. Eng. Chem. Res.*, **45**, 8723 (2006).
8. H. Zhao, J.-X. Wang, Q.-A. Wang, J.-F. Chen and J. Yun, *Ind. Eng. Chem. Res.*, **46**, 8229 (2007).
9. J. Bałdyga, D. Kubicki, B. Y. Shekunov and K. B. Smith, *Chem. Eng. Res. Des.*, **88**, 1131 (2010).
10. S. Salmaso, N. Elvassore, A. Bertucco and P. Caliceti, *J. Pharm. Sci.*, **98**, 640 (2009).
11. E. Reverchon, R. Adami, S. Cardea and G. Della Porta, *J. Supercrit. Fluids*, **47**, 484 (2009).
12. M.-W. Park and S.-D. Yeo, *Chem. Eng. Res. Des.*, **90**, 2202 (2012).
13. S.-D. Yeo and J.-C. Lee, *J. Supercrit. Fluids*, **30**, 315 (2004).
14. D. A. Weingaertner, S. Lynn and D. N. Hanson, *Ind. Eng. Chem. Res.*, **30**, 490 (1991).
15. J. Chen, C. Zheng and G. A. Chen, *Chem. Eng. Sci.*, **51**, 1957 (1996).
16. H. Zhao, J. Wang, H. Zhang, Z. Shen, J. Yun and J. Chen, *Chin. J. Chem. Eng.*, **17**, 318 (2009).
17. G. Tosun, 6th European Conference on Mixing (1988).
18. B. K. Johnson and R. K. Prud'homme, *AIChE J.*, **49**, 2264 (2003).
19. A. Mersmann, *Chem. Eng. Process.*, **38**, 345 (1999).
20. H. Grénman, E. Murzina, M. Rönnholm, K. Eränen, J.-P. Mikkola, M. Lahtinen, T. Salmi and D. Y. Murzin, *Chem. Eng. Process.*, **46**, 862 (2007).
21. D. Rao, A. Bhowal and P. Goswami, *Ind. Eng. Chem. Res.*, **43**, 1150 (2004).
22. G. Akay, L. Tong and R. Addleman, *Ind. Eng. Chem. Res.*, **41**, 5436 (2002).
23. J.-F. Chen, Y.-H. Wang, F. Guo, X.-M. Wang and C. Zheng, *Ind. Eng. Chem. Res.*, **39**, 948 (2000).
24. V. Hessel, H. Löwe and F. Schönfeld, *Chem. Eng. Sci.*, **60**, 2479

(2005).
25. J. d. Mello and A. d. Mello, *Lab Chip*, **4**, 11 (2004).
26. S. Taghavi-Moghadam, A. Kleemann and G. Golbig, *Org. Process Res. Dev.*, **5**, 652 (2001).
27. W. Ehrfeld, CHIMIA *Int. J. Chem.*, **56**, 598 (2002).
28. P. Patil, G. Khairnar and J. Naik, *Chem. Eng. Res. Des.*, **104**, 98 (2015).
29. Y. He, Y. Huang and Y. Cheng, *Cryst. Growth Des.*, **10**, 1021 (2010).
30. Z. Liu, Y. Huang, Y. Jin and Y. Cheng, *Microfluid. Nanofluid.*, **9**, 773 (2010).
31. W. Wang, S. Zhao, T. Shao, Y. Jin and Y. Cheng, *Chem. Eng. J.*, **192**, 252 (2012).
32. M. Kakran, N. G. Sahoo, I. L. Tan and L. Li, *J. Nanopart. Res.*, **14**, 757 (2012).
33. Y. He, Y. Huang, W. Wang and Y. Cheng, *Chem. Eng. J.*, **168**, 1021 (2011).
34. P. Valeh-e-Sheyda, M. Rahimi, A. Parsamoghadam and H. Adibi, *J. Taiwan Inst. Chem. Eng.*, **46**, 65 (2015).
35. P. Valeh-e-Sheyda, M. Rahimi, H. Adibi, Z. Razmjou and H. Ghasempour, *Chem. Eng. Process*, **91**, 78 (2015).
36. S. C. Ferreira, R. Bruns, H. Ferreira, G. Matos, J. David, G. Brandao, E. P. da Silva, L. Portugal, P. Dos Reis and A. Souza, *Anal. Chim. Acta*, **597**, 179 (2007).
37. J. Hunter, J. Hunter and G. Box, Wiley series in probability and mathematical statistics (1978).
38. G. E. Box and K. Wilson, *J. R. Stat. Soc. Series B*, **13**, 1 (1951).
39. G. E. Box and D. W. *Technometrics*, **2**, 455 (1960).
40. A. S. Souza, W. N. L. dos Santos and S. L. C. Ferreira, *Spectrochim. Acta, Part B*, **60**, 737 (2005).
41. D. C. Montgomery, John Wiley & Sons (2008).
42. S. M. Agnihotri and P. R. Vavia, *Biol. Med.*, **5**, 90 (2009).
43. S. Chopra, G. V. Patil and S. K. Motwani, *Eur. J. Pharm. Biopharm.*, **66**, 73 (2007).
44. Y.-L. Li, Z.-X. Fang and J. You, *J. Agric. Food Chem.*, **61**, 1464 (2013).
45. N. Celebi, N. Yildiz, A. S. Demir and A. Calimli, *J. Supercrit. Fluids*, **47**, 227 (2008).
46. Y. W. Guozhong Cao, 2nd Ed., World Scientific, London (2011).
47. M. Kakran, N. G. Sahoo, L. Li, Z. Judeh, Y. Wang, K. Chong and L. Loh, *Int. J. Pharm.*, **383**, 285 (2010).
48. M. E. Matteucci, M. A. Hotze, K. P. Johnston and R. O. Williams, *Langmuir*, **22**, 8951 (2006).
49. H.-X. Zhang, J.-X. Wang, Z.-B. Zhang, Y. Le, Z.-G. Shen and J.-F. Chen, *Int. J. Pharm.*, **374**, 106 (2009).
50. A. Sengupta, P. D. Kamble, J. K. Basu and S. Sengupta, *Ind. Eng. Chem. Res.*, **51**, 147 (2011).
51. Zetasizer Nano Series, Nano Series, User Manual. MAN0317. Issue 1.1. (2004).
52. A. A. Thorat and S. V. Dalvi, *Cryst. Eng. Comm.*, **16**, 11102 (2014).
53. P. R. K. Mohan, G. Sreelakshmi, C. V. Muraleedharan and R. Joseph, *Vib. Spectrosc.*, **62**, 77 (2012).
54. B. E. Rabinow, *Nat. Rev. Drug Discovery*, **3**, 785 (2004).
55. J. Sun and S. Simon, *Thermochim. Acta*, **463**, 32 (2007).
56. S. Kim, W. K. Ng, Y. Dong, S. Das and R. B. Tan, *J. Food Eng.*, **108**, 37 (2012).